On the use of solubility parameters to investigate phase separation-morphology-mechanical behavior relationships of TPU

Raïssa Gallu, Françoise Méchin, Florent Dalmas, Jean-François Gérard, Rémi Perrin, Frédéric Loup

▶ **To cite this version:**

Raïssa Gallu, Françoise Méchin, Florent Dalmas, Jean-François Gérard, Rémi Perrin, et al.. On the use of solubility parameters to investigate phase separation-morphology-mechanical behavior relationships of TPU. Polymer, 2020, 207, pp.122882. 10.1016/j.polymer.2020.122882 . hal-02926028

HAL Id: hal-02926028
https://hal.science/hal-02926028v1

Submitted on 31 Aug 2020

HAL is a multi-disciplinary open access archive for the deposit and dissemination of scientific research documents, whether they are published or not. The documents may come from teaching and research institutions in France or abroad, or from public or private research centers.

L'archive ouverte pluridisciplinaire **HAL**, est destinée au dépôt et à la diffusion de documents scientifiques de niveau recherche, publiés ou non, émanant des établissements d'enseignement et de recherche français ou étrangers, des laboratoires publics ou privés.

On the use of solubility parameters to investigate phase separation-morphology-mechanical behavior relationships of TPU.

Raïssa Gallu[1,2*], Françoise Méchin[1], Florent Dalmas[2], Jean-François Gérard[1], Rémi Perrin[3], Frédéric Loup[4]**

[1] Univ Lyon, INSA Lyon, CNRS, UMR 5223 IMP, F-69621, Villeurbanne, France.
[2] Univ Lyon, INSA Lyon, CNRS, MATEIS, UMR5510, F-69621, Villeurbanne, France.
[3] Soprema Co., 14 rue de Saint Nazaire, 67100 Strasbourg, France.
[4] Eiffage Infrastructure Co., Corbas, France.

[*] Corresponding author : Email address gallu.raissa@gmail.com
[**] Corresponding author : Email address francoise.mechin@insa-lyon.fr

Abstract:

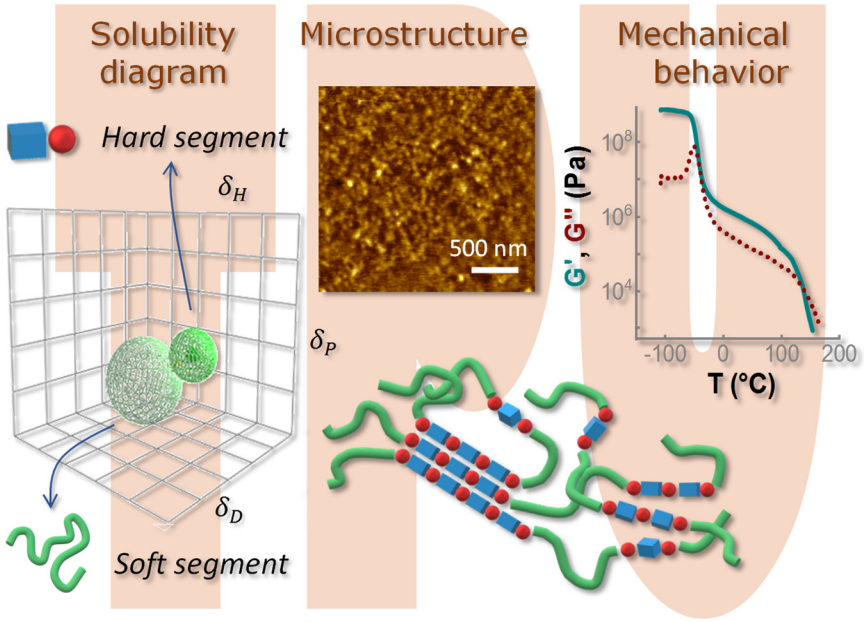

This study proposes a thorough investigation, especially based on thermodynamics, to predict phase separation in a linear thermoplastic polyurethane, denoted TPU, prepared from fatty acid-based soft segments and MDI (4,4'-methylene bis(phenyl isocyanate))/BDO (1,4-butanediol) hard segments and specially designed for bitumen modification. Hansen' solubility parameters (HSP) of both segments are evaluated to predict their compatibility. The later ones are evaluated either individually from the corresponding segment synthesized separately or from a decomposition of the solubility diagram of the TPUs into two distinct spheres. In a second step, phase separation is experimentally analyzed by combining differential scanning calorimetry, microscopy techniques, and small angle X-ray scattering (SAXS). The microstructure of the TPUs is described considering one soft phase

made of polyol chains and short miscible hard segments and a hard phase organized as semi-crystalline nanodomains either dispersed or assembled as ramified (nano)objects within the soft phase. The dynamic mechanical properties of the TPUs can be explained by the presence of such well-defined hard domains in the structure of the TPU, acting as reinforcing fillers while maintaining a thermoplastic elastomer mechanical behavior to the TPU above the glass transition of the continuous soft phase.

---

1. Introduction

Polyurethane polymers are widely used in consumers daily life products and find applications in a wide range of comfort and insulation products[1], thanks to the versatility of their macromolecular architecture allowing them to be categorized as thermosets, thermoplastics, or elastomers**.** Thermoplastic polyurethanes, TPUs, usually come from the combination of three components, i.e. a polyol or macrodiol having a high molar mass (up to 3,000 $g.mol^{-1}$), a diisocyanate, and a diol or chain extender of low molar mass[1,2]. In order to reduce petrochemical polymers production, TPUs from biobased materials have known a high development in the last years. The biobased building blocks could be provided by the polyol, e.g. derived from dimer fatty acids[1], but also from the chain extender, such as isosorbide which has known a high development in polyurethanes in recent years[3,4], and even by the diisocyanate itself, as an example with the fatty acid-derived diisocyanate dimeryl diisocyanate (DDI)[3,5]. With the rise of the biobased raw materials available for the synthesis of TPUs, polymers of high biobased content can now be produced.

TPUs exhibit soft and hard blocks in their structure, provided by the reaction of the polyol with the diisocyanate and of the diisocyanate with a chain extender, respectively[1,2]. Depending on their macromolecular architecture, in relation with their synthesis procedure, thermoplastic polyurethanes can organize as segmented pseudo-block copolymers, sometimes with (micro)phase separation between soft and hard segments. This property can first be revealed by means of thermal analysis like differential scanning calorimetry (DSC), which can evidence the glass transitions and possible meltings relative to each phase, and can give a first idea of their purity from the values of the associated temperatures.[6,7]. In addition, Camberlin and Pascault reported that it was possible to precisely estimate from DSC the segregation degree between both type of segments, based on the change of heat capacity at T_g[8].

As thermoplastic elastomers (TPEs), above the α main mechanical relaxation, associated to the glass transition of the soft phase, TPUs show a rubbery plateau before the flow of the polymer occurring as the hard segments aggregates collapse. As a consequence, the mechanical properties depend on the initial components used which control the 'quality' of the phase separation between blocks, as shown for example with difference of thermomechanical properties observed for TPUs synthesized either with MDI diisocyanate

or toluene diisocyanate (TDI)[9]. The hard segments content has also a large influence on the phase separation, and particularly on the modulus at the rubbery plateau[10].

Other characterization techniques are commonly used to reveal phase separation such as transmission electron microscopy, TEM, atomic force microscopy, AFM, or X-ray scattering[11]. Based on microstructure analyses, the phase separation relates with the presence of hard domains, either within spherulite-like structures[12], globular structures [4,13,14], or combinations of both[15]. At nano-scale, X-ray analysis provides information about the organization of the hard domains in the structure of the soft phase, such as the crystalline form[16] or interdomain spacing as highlighted by Aneja and Wilkes[17]. These authors reported interdomain spacing of 10.6 nm for a polyurethane prepared from poly(tetramethylene oxide) soft segments and 1,4-butanediol extended piperazine-based hard segments.

The specific characteristic of thermoplastic polyurethanes to organize as segmented block copolymers allows them to behave as TPEs, i.e. to display a constant rubbery modulus above the T_g of the soft continuous phase as crosslinked rubbers.

The ability of TPEs to phase segregate results from the thermodynamic incompatibility between the two blocks. Indeed, considering the block copolymers as a binary blend of soft and hard blocks, the system can be described based on Flory-Huggins' theory[18,19] by the change of free enthalpy ,ΔG_M, expressed in the following equation by:

$$\frac{\Delta G_M}{kT} = \frac{\Phi_A ln \Phi_A}{v_A N_A} + \frac{\Phi_B \, ln \, \Phi_B}{v_B N_B} + \chi'_{AB} \Phi_A \Phi_B \qquad \text{(Eq.1)}$$

with N_i being the number of monomers in the chain i, v_i the volume of each monomer on chain i, Φ_i the volume fraction of block i, and χ_{AB} the Flory interaction parameter, defined as follows:

$$\chi_{AB} = V_{ref} \times \frac{(\delta_A - \delta_B)^2}{RT} \qquad \text{(Eq.2)}$$

where V_{ref} is the reference volume, and δ_A, δ_B the Hildebrand solubility parameters[18] of blocks A and B, respectively. The solubility parameter is defined by:

$$\delta = \left(\frac{E}{V}\right)^{\frac{1}{2}} \qquad \text{(Eq.3)}$$

where V is the molar volume and E the energy of vaporization of the component. The required condition to obtain a miscible blend, meaning no phase separation, implies $\Delta G_M < 0$. Phase separation is expected well-defined in block copolymers such as styrene-butadiene-styrene (SBS), a common polymer modifier for bitumen, where both blocks show rather different solubility parameters[20].

The interaction parameter, χ, (calculated from the solubility parameters) allows to describe the phase diagram in block copolymers that usually show a LCST-type (lower critical solution temperature) behavior. The diagram describes the transition of a homogeneous disorganized system to a mesophase structure, where various types of nanostructures, such as spheres, cylinders, or lamellae coexist, depending on the block compositions[21]. By extension, this can also apply to the TPU morphology based on hard and soft segments.

As an example, for polyurethanes based on poly(propylene oxide) (PPO) and various hard segments (MDI/BDO, MDI/3,5-diethyltoluene diamine), a high solubility parameter of the hard segments leads to a high interaction parameter and an organized structure is observed for the hard domains even for a lower hard segment content[22]. This comes from the high difference in solubility parameters between the soft PPO segment and the hard segments (17 $MPa^{1/2}$ vs. more than 22 $MPa^{1/2}$, respectively), leading to a high degree of phase separation which can be also favored by the ability of the hard chains to self-assemble and organize. Hard segments having urea functions are even more capable of self-organizing, due to the occurrence of additional hydrogen bonds[23], and display even higher solubility parameters. As a consequence, a highly phase separated polymer containing well organized hard domains relates with a higher modulus in the rubbery state[22].

Camberlin and Pascault[24] pointed out that the quality of phase separation is also dependent on the architecture of the polyol (precursor of the soft segments) which is considered by estimating interaction parameters in polyurethanes having MDI/BDO hard segments. With those type of HS, they reported an interaction parameter for a PPO-based soft segment $\chi = 2.8$, whereas with the same hard segments the corresponding hydrogenated (1,2)-polybutadiene soft segment displayed an interaction parameter $\chi = 4.7$. Although the authors could calculate a critical value of $\chi_{cr} = 0.34$ (that takes into account the low polymerization degree of the considered segments) above which no miscibility should theoretically be possible, the system based on PPO yet displayed high miscibility presumably forced by the existence of covalent bonds between both types of segments, in contrast to that with polybutadiene soft segments that was definitely immiscible.

In the late 60s, Hansen has described the global solubility parameter, δ, as the combination of three components reflecting dispersive (London) (δ_D), polar (δ_P), and hydrogen bond (δ_H) interactions[25],[26,27]:

$$\delta^2 = \delta_{TOT}^2 = {\delta_D}^2 + {\delta_P}^2 + {\delta_H}^2 \qquad \text{(Eq.4)}$$

The components δ_D, δ_P, and δ_H are named Hansen' Solubility Parameters, HSP. Hansen also defined a 3D solubility diagram $(\delta_D, \delta_P, \delta_H)$ where a solubility sphere having a radius R_0 can be defined for large molecules. The analysis is based on solubilization tests in solvents of known HSP, with a sphere that encompasses the good solvents of the component in the 3D space[28]. Compatibility between two compounds can be estimated based on their HSP values : compounds with close HSP and with a low distance between centers of their

respective solubility spheres are expected to display a good mutual affinity. This implies that the solubility spheres of the components are overlapping. The distance R_a between centers of the solubility spheres of two components named as 1 and 2, is given by:

$$R_a^2 = 4(\delta_{D1} - \delta_{D2})^2 + (\delta_{P1} - \delta_{P2})^2 + (\delta_{H1} - \delta_{H2})^2 \quad \text{(Eq.5)}$$

For a given component/solvent pair, the considered solvent would exhibit strong affinity with the component for a very low value of R_a (inferior to R_0, the radius of the solubility sphere). In this case, the solvent coordinates are expected to be inside the component solubility sphere. However, when considering two different components, a value of R_a = 8 $MPa^{1/2}$ is usually considered as the upper limit for compatibility [25].

In the last decades, literature has reported several works dealing with the solubility of polymers and other compounds[25]. First records were on the use of turbidimetric titration to estimate HSP of polymers such as polystyrene[29] (PS), polyurethanes (combined with intrinsic viscosity)[30] or polyols[31]. Turbidimetric titration has also been used to calculate bitumen solubility parameters[32]. In the last years, inverse gas chromatography proved to be an accurate method to determine HSP of block copolymers such as poly(ethylene-co-vinyl acetate) [33], or SBS[34]

Others reported the use of solvent mixtures and a viscosimetric method to determine HSP in order to calculate the interaction parameter in block copolymers[35]. Although these authors found discrepancies between theoretical and experimental values, the tendency of the polymer to phase separate is definitely higher if the interaction parameter is high.

Another method consisting in simple solubility tests in various solvents combined with calculations by a dedicated software was used to estimate HSP on polystyrene and polybutadiene[20] or bitumen[36]. In recent years, Bouteiller *et al*. reported the determination of HSP and solubility spheres with the new HSPiP software[28] (allowing to calculate or predict HSP based on a solvent database and algorithm) for low molar mass organogelator molecules and went even further with the determination of a gelation sphere[37,38].

HSP have also been used to predict miscibility in polymer blends, as reported by David and Sincock[39]. Furtwengler et *al*., as well as Zhang and Kessler[40,41] used Hansen' solubility spheres diagram obtained with HSPiP software to estimate compatibility between polyols to make stable emulsions with a view to manufacturing foams. This method has also been reported by Redelius to study compatibility of bitumen with different polymers, such as SBS, polyethylene sulfide or polyether sulfone[36].

Mieczkowski showed that the solubility parameters of the polyurethane polymers are very dependent on the soft segment molecular architecture[30]. In fact, a poly(ethylene adipate)(PEA)-based polyurethane proved to be more polar than the corresponding PPO-based polyurethane.

Conventional soft blocks considered for the synthesis of TPUs usually show total solubility parameters lower than 20 $MPa^{1/2}$, while hard blocks display higher solubility values. As an

example, Table 1 reports the solubility parameter of a range of soft and hard segments often considered for the synthesis of polyurethanes.

Table 1: Solubility parameter of soft and hard segments commonly considered in polyurethanes and polyurethane-ureas[1,22–24,42,43]

Soft segment	δ ($MPa^{1/2}$)	Hard segment	δ ($MPa^{1/2}$)
Polydimethylsiloxane (PDMS)	15.6	MDI/EG (ethylene glycol)	21.0
Poly(ethylene butylene) (PEB)	16.2	Isophorone diisocyanate/1,4-butanediol (IPDI/BDO)	21.2
Polyisobutylene (PIB)	16.4	Hexamethylene diisocyanate/ 1,4-butanediol (HDI/BDO)	21.9
Polybutadiene (PB)	16.8	4,4′-methylene bis(phenyl isocyanate /4,4′-diaminodiphenyl ether (MDI/DDE)	24.3
Polybutylene adipate (PBA)	17.0	4,4′-methylene bis(phenyl isocyanate/3,5-diethyltoluenediamine (MDI/DETDA)	24.9
Polycaprolactone (PCL)	17.0	4,4′-methylene bis(phenyl isocyanate/1,4-butanediol (MDI/BDO)	22 - 27
Poly(tetramethylene oxide) (PTMO)	17.6	MDI/EDA	23 - 29
Poly(propylene oxide) (PPO)	18.9		
Poly (ethylene adipate) (PEA)	19.8		
Poly(ethylene oxide) (PEO)	20.2		

The present study reviews the synthesis of a TPU with a soft segment derived from fatty acids. TPUs derived from such polyols and MDI-BDO hard segments indeed already proved

to be particularly well suited to the manufacture of bituminous binders[44]. The solubility parameters of the soft segments are evaluated and compared to those of the hard segment in order to predict phase separation in the TPU based on thermodynamic incompatibility of the segments. Phase separation is also evaluated by using conventional methods such as differential scanning calorimetry and morphology characterization techniques (AFM, TEM, and SAXS). From these results, relationships between thermomechanical state and physical behaviors, i.e. rheology and dynamic mechanical properties (DMA), of the investigated TPU are established. This work is the first step of a more global study aiming to optimize the blends of the present TPU with bitumen, by establishing the interactions occurring between the polymer's blocks and the bitumen's fractions, and consequently better understanding the resulting mechanical and morphological properties of the material.

2. Materials and methods

2.1. Materials

The polyester polyol Radia 7285 based on fatty acid was provided by Oleon Co., the diisocyanate 4,4'-methylene bis(phenyl isocyanate) (MDI), and the chain extender, 1,4-butanediol (BDO), were provided by Sigma Aldrich Co. The solvents used were also provided by Sigma Aldrich Co.

The polyol was used to synthesize TPUs along with MDI diisocyanate and BDO as chain extender. A two-step synthesis was used consisting in the formation of a pre-polymer in the first step, made with excess of MDI and the polyol. The reaction of MDI with the polyol gives what is commonly denoted as soft segments (SS) displaying a glass transition below 0°C. In the second step, the addition of the chain extender BDO leads to the formation of hard segments (HS) coming from its reaction with the prepolymer that contains isocyanate-terminated oligomers and residual MDI. TPUs with different HS contents, ranging from 8 to 30 wt%, were synthesized (throughout this work the HS content is defined as the overall (MDI + BDO)/(polyol + MDI + BDO) weight ratio). The following code is used for the TPU: for TPU without added chain extender (8wt% HS, see below), TPU 8; and for TPU with 13wt%, 15wt%, 20wt% 25wt% and 30wt% HS, TPU 13, TPU 15, TPU 20, TPU 25 and TPU 30, respectively. It can be noticed that the polyol contains hexanediol chain ends, which after reaction provide what can be viewed as short MDI/HDO pseudo hard segments, even when no additional chain extender is used, whose ratio in the TPU is estimated at 8wt%. Taking those moieties into account can modify the calculated HS content, especially when the used amount of BDO is very low (see below, § TPU morphologies).
In the first step of the synthesis, the procedure consisted in adding the polyester polyol and the required excess of MDI diisocyanate in a 300 mL closed reactor thermoregulated by an oil bath at 80°C. The mixture was placed under nitrogen atmosphere and stirred at 600 rpm for 50 min. A precise amount of chain extender BDO was then added with a syringe and the mixture stirred at 1,000 rpm during 1 min, then at 600 rpm for about 10 min according to the viscosity value. If the mixture became too viscous before this total duration, stirring was

stopped and the polymer was poured on a metallic plate in an oven at 80°C for 12 h to proceed polymerization and post-curing. The polymer was then put between two metallic plates under a hot press at 110°C, 40 bar pressure for 1 h, and cooled at room temperature to process TPU specimens of 2 mm thickness.

MDI/BDO polymer considered in the present study as a model of pure HS, were synthesized by solution polymerization in a 250 mL flask in tetrahydrofuran. The reaction was catalyzed by 0.01 wt% of dibutyltin dilaurate for 24 h under magnetic stirring at 65°C (reflux). After 24h, the obtained turbid solution was cooled down to room temperature under air before the addition of distilled water, which allowed the precipitation of the hard segment. The precipitated hard segment was washed several times and filtered on a Buchner filter to obtain a white powder which was finally dried in an oven at 100°C for 4 h. One can mentioned that such a protocol probably implied that the recovered hard chains displayed a rather small molar mass, since their growth was supposed to be stopped by precipitation (but due to their insoluble character, the measurement of their molar mass by SEC was not possible).

2.2. Methods

Dynamic mechanical analysis (DMA) was made in torsion mode on a homemade pendulum under inert atmosphere (helium) at 600 mbar from -120 to 130°C with a heating rate of 1 $K.min^{-1}$. The test was performed at a constant frequency of 1 Hz and low strain amplitude (10%) on parallelepipedic coupons (2 x 6 x12 mm^3).

Rheological properties of TPUs were measured using an ARES rheometer from TA Instruments Co. at 1Hz from 80 to 180°C considering a plate-and-plate geometry (25 mm diameter, 2 mm gap) and 2% strain amplitude.

Differential scanning calorimetry tests were carried out using a Q20 TA Instrument calibrated with Indium. Hermetic aluminum pans were used to seal TPU samples of 5-7 mg which underwent a first cooling stage from room temperature to -80°C, followed by a heating ramp of $10K.min^{-1}$ up to 240°C. The specimens were submitted to a nitrogen flow rate of 50 $mL.min^{-1}$. The value of the glass transition temperature is given at the onset point and the variation of heat capacity ΔC_P is calculated by the TA Instruments software at the T_g midpoint.

^1H NMR spectroscopy was performed using a Bruker Advance III 400 at 298 K with deuterated chloroform ($CDCl_3$) as solvent. The ^1H NMR spectra were recorded at 400 MHz with an acquisition time of 2 s, a pulse delay of 4 s, and for 128 scans.

Size Exclusion Chromatography was carried out on a Shimadzu apparatus equipped with refractive index and viscometer detectors and calibrated with polystyrene standards. Tetrahydrofuran was used as eluent on a set of columns Malvern Viscotek maintained at 35°C. The pore size of the columns was 0.5, 1, and 2 μm. Samples with concentrations of 1 up to 3 $g.L^{-1}$ were analyzed. The molar mass was determined using a polystyrene calibration curve on OmniSEC software.

MALDI-TOF measurements were conducted on a Voyager-DE PRO from Applied Biosystems equipped with a N_2 laser (λ = 337 nm) with dithranol as a matrix. The spectra were recorded in linear and reflectron modes. An external calibration was performed with a Sequazyme™ peptide mass standards kit (AB Sciex). The matrix solution (10 $g.L^{-1}$ in chloroform) was mixed with the polyol solution (10 $g.L^{-1}$ in chloroform) and a NaI solution (10 $g.L^{-1}$ in acetone) with a volumetric ratio 9:1:1, and 1 μL of this blend deposited and co-crystallized on the MALDI plate.

Hansen' solubility parameters were evaluated using HSPiP® sofware[28] after testing the polymer solubility in various solvents (choosing an increment value of 1 for soluble situation and a value of 0 for non-soluble situation). Mixtures of solvents were also used by using the Optimizer program provided by the software. The measurement was based on Hansen's calculation of the solubility parameter and led to a three dimension (3D) diagram (δ_D; δ_P; δ_H) of solubility parameters with a solubility sphere encompassing the good solvents for the considered compound.
Different solvents of various HSP values were chosen with the aim to fill the entire 3D space diagram (supporting information Table S1). Thus, samples of 35-40 mg were placed in a small flask which was filled with 3 mL of solvent. The mixture was then stirred under ultrasound waves at room temperature (between 25 and 30°C) for 30 minutes. Solubility power of the considered solvent was evaluated after few minutes, 24h, and three weeks. Since the solubility can evolve with time, the final solubility (after three weeks) is chosen. The HSPiP software provided HSP values, the whole (total) solubility parameter, δ_{TOT}, and the radius of the solubility sphere, R_0, for the considered polymer. Distances and sphere solubility overlapping between two components, R_a, were determined from their HSP values using the distance tool of the software.

Static small angle X-ray scattering (SAXS) and ultra-small angle X-ray scattering (USAXS) experiments were performed at room temperature with an energy beam of 12.46 keV on the ID2 beamline of the European Synchrotron Radiation Facility (ESRF), Grenoble (France). For SAXS measurements, the sample-detector distance was 1 m and the exposure time was set at 0.5 s while for the USAXS investigations, the distance between sample and detector was 10 m and the exposure time was set at 0.05 s. The SAXS/USAXS two-dimensional (2D) patterns of all synthesized TPUs did not show any preferential orientation; for this reason, the I=f(q) data presented are obtained from the azimuthal average of the scattering pattern from which all the necessary data corrections have been applied

(background scattering subtraction and sample thickness correction). In addition, a Kratky plot presented in supporting information allowed to facilitate the identification of correlation peaks between HS nodules.

Samples for transmission electron microscopy, TEM, were prepared by cryo-ultramicrotomy at -80°C on a UC7 Leica microtome device using two diamond knifes, the first one for the pyramid preparation and the second for cutting slices of 100 nm thickness. Observations were conducted on a Philips CM120 at an acceleration voltage of 120kV at ambient temperature.

Atomic force microscopy (AFM) was performed with a Dimension 3100 AFM device connected to a NanoScope V scanning probe controller (Bruker Instruments, Plainview, NY). The samples for AFM were prepared by cryo-microtomy at -80°C as for TEM. All images were obtained at ambient temperature in tapping mode using a pointprobe-plus® silicon (PPP-NCH) from Nanosensors with a high resonance frequency (ca. 300 kHz). Only phase images (highlighting a hard/soft contrast) after treatment with Gwyddion freeware[45] are discussed in the present paper and the corresponding height images are shown in supporting information (Figure S6). Indeed, in addition to artifacts from microtomy (scratches, folding…), the AFM height images slightly highlight (with a lower contrast) the same morphological features as phase images, because of thermal expansion difference between soft and hard phases that causes a variation in topography once frozen samples are brought to RT again.

3. Results & Discussion

3.1. Physico-chemical characterization of initial building blocks of TPU

The polyester polyol Radia 7285 supplied by Oleon Co. obtained from dimerization and esterification of rapeseed oil is 80 wt% biobased. This polyol displays a very high molar mass dispersity and the calculation of the average molar mass by ^{1}H NMR gave a lower value of 3,200 g.mol^{-1}. This latter value is in a good agreement with the bi-functionality of the polyol and the hydroxyl number of 35.8 mg KOH.g^{-1} provided by the supplier. It is well known that dimerization of fatty acids can lead to several chemical structures, either cyclic, polycyclic, acyclic, or even aromatic[46,47]. Rapeseed oil contains mainly oleic and linoleic acids[48] which can lead to dimerization which produces mainly cyclic dimers. Based on NMR and MALDI-TOF mass spectrometry analyses (supporting information, Figure S1-2), a possible molecular structure for this polyol has been proposed based on dimer fatty acid and hexanediol (HDO) (see Figure S1 in SI). Other polyols considered for the synthesis of thermoplastic polyurethanes were also obtained from rapeseed oil as reported by Bueno-Ferrer et *al*[49].

At low temperature, DSC analyses of the TPU samples (Figure 1) show *i*/ a glass transition (T_g) ascribed to the co-operative and long distance molecular motions, i.e. T_g region

of the TPU soft segments close to – 54°C, *ii/* followed by a second calorimetric phenomenon occurring in the 30-60°C, depending on the TPU HS content, which can therefore be related somehow to the hard segments-rich domains (glass transition, enthalpy relaxation).

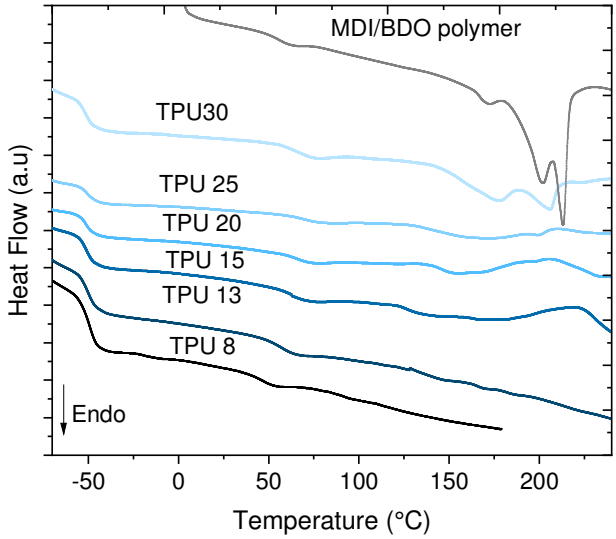

Figure 1. DSC scans of various TPUs based on different MDI/BDO hard segment contents and of i.e. MDI-BDO polymer.

It should be noticed that increasing HS content doesn't influence the glass transition temperature of the soft phase, contrary to what could be observed if both segments were partially miscible and meaning that the hard segment chains lie rather outside the soft segment-rich region. Otherwise, increasing amounts of dissolved hard segments would probably induce a notable increase in the soft Tg. This constant value of Tg rather suggests a high degree of phase separation between HS and SS in the TPUs. In order to confirm this assumption, the phase separation degree was evaluated by considering the difference of isobaric heat capacity, ΔC_p, at the glass transitions of the soft segments for the different TPUs.

As expected, Figure **2** shows that ΔC_p at the T_g of the soft segments decreases when increasing the HS content of the TPU. This decrease can obviously be explained by the decreasing content of soft segment involved in this transition.

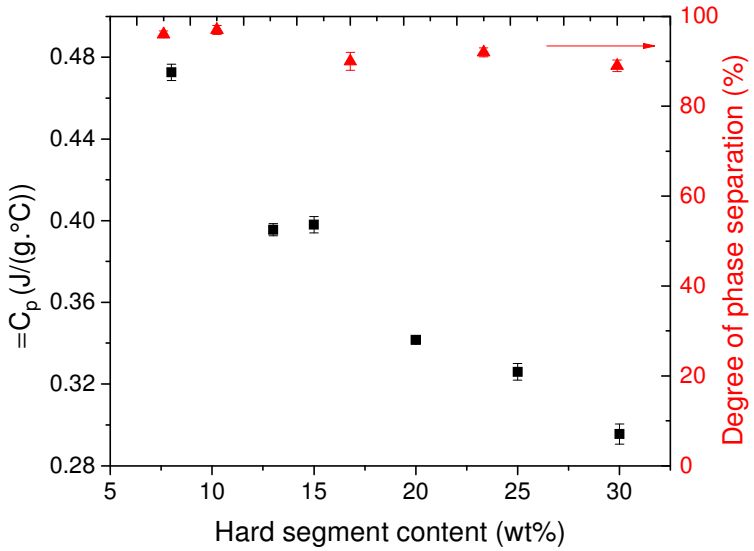

Figure 2. Change of heat capacity, ΔC_p, at the glass transition of the soft phase (■) and of the corresponding phase separation degree (▲), as a function of hard segment content.

Based on the work of Camberlin and Pascault[8], an attempt to estimate the segregation degree of the TPU was proposed by using the following equation:

$$\text{Segregation degree} = \frac{\Delta C_{p2}}{\Delta C_{p1}} \qquad \text{(Eq.6)}$$

with ΔC_{p1}, the change of the isobaric heat capacity for the TPU without MDI/BDO hard segments and ΔC_{p2} defined as the change of the isobaric heat capacity at the T_g of the soft segment per grams of soft phase in the TPUs ($\Delta C_{p2} = \frac{100\Delta C_p}{(wt\% \ SS)}$). As shown in Figure **2**, all the TPUs display a very high degree of phase separation, as more than 10 wt% of the soft segments aren't involved in the glass transition of the soft phase but could be trapped in the hard domains. However, this already suggests that the affinity between the soft and hard segments of this TPU series is not very high.

A second calorimetric event then occurs in the 30-60°C, depending on the TPU HS content. Several physical phenomena could be behind this transition, including the Tg of a hard phase, H-bond interactions, annealing-induced order or even microphase mixing. Such intermediate events are very often detected for most segmented polyurethanes and have been the object of numerous and sometimes inconsistent interpretations in the literature[50]. For MDI/BDO hard segments, literature reports a glass transition temperature close to 107°C in a polyurethane based on hydrogenated polybutadiene soft segment[10], that is much

higher than the value observed in this study, therefore the phenomenon should presumably not be attributed only to the Tg of the HS. The breakage of hydrogen bonds between urethane NHs and ester carbonyls (present in our polyol) was mentioned in the past as another possible cause[23,51]. Finally, an amorphous interphase composed of mixed soft and hard segments might exist near domain boundaries. Indeed, a similar study from Cuvé et *al*. dedicated to TPUs containing hydrogenated polybutadiene soft segments, highlighted the presence of a broad phenomenon (that they attributed to the HS glass transition) at 34 or 51°C (from first DSC heating scans) depending on the hard segment nature used (more precisely chain extender nature)[52]. Blache [4] also observed a similar event between 55 and 60°C for TPUs based on a polyol close to ours, but did not conclude on its precise origin.

Considering in more details the onset temperature values of this event, it appears that they regularly increase from 39 to 61°C with the HS content in the TPU up to 25 wt% (Figure 3). Similar results were reported e.g. for TDI/BDO hard segments in literature[53,54]. Increasing HS content in the formulation leads to longer HS chains on average[55,56], therefore their length could be the key parameter influencing this temperature, together with the length dispersity[53]. Here the width of this thermal event lies between 14 to 20°C, suggesting a broad distribution of molar masses of the hard segments chains.

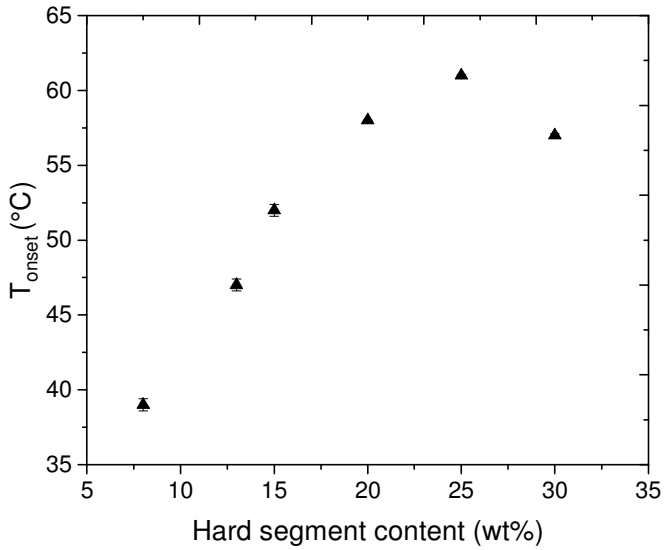

Figure 3. Onset temperature of the intermediate thermal event as a function of hard segment content in the TPUs.

At higher temperature, the neat hard segment as well as TPUs with high HS contents show melting endotherms occurring from 160 to 200°C (Figure 1). Regarding the neat MDI/BDO HS, which is known to be semi-crystalline[57,58] (as confirmed by WAXS, see supporting information Figure S3), melting endotherms are observed at 170, 200, and 213°C. These three endotherms suggest either the presence of several types of crystalline morphisms or that some amorphous hard segments are trapped inside organized zones. Indeed,

Blackwell and Lee reported polymorphism of MDI/BDO hard segments with the presence of two crystalline structures, denoted as extended and contracted, displaying two different thermal behaviors[16]. The extended structure displays a melting endotherm from 170 to 180°C and the contracted one, from 205 to 215°C, therefore in agreement with our results.

For TPU 30, two melting endotherms are present, i.e. at 178 and 206°C, suggesting also different crystalline organizations in the polymer in agreement with Koberstein and Stein that evidenced two melting endotherms for a polyurethane based on MDI/BDO hard segment[59]. Other studies came to the same conclusions with polyurethanes containing MDI/hexanediol (HDO) hard segments[16,60].

However, some researchers reported that the presence of multiple endotherms in TPUs were due to different degrees of mixing of soft segments in hard domains[61], while others explained it by successive melting and recrystallization of some hard segments[50,62]. In the case of this study, recrystallization cannot be evoked as increasing the heating rate resulted also in the occurrence of two melting endotherms (see Figure S4 in SI). Then, based on all of the previous results, one can assume that the two endotherms observed are due to combined phenomena: *i*/ mixing of soft and short hard segments trapped in crystalline hard domains, and *ii*/ different crystalline morphisms of the hard segments themselves.

To go further, thermodynamic aspects involving Hansen solubility parameters (HSP) and the solubility diagrams in the 3D space ($\delta_D, \delta_P, \delta_H$) are now considered to explain the occurrence of phase separation in the TPU. From a macromolecular point of view, TPU materials can be considered in two different ways. The first one considers independently the HSP of both constituents of the polymer assumed to be the pristine polyol Radia 7285 and the MDI/BDO polymer (which can be considered as neat hard segments). The second approach considers the whole TPU macromolecule as a single constituent. Thus, HSP were evaluated using solvent tests and HSPiP software based on the Hansen' algorithm. For the polyol, turbidimetric titration with mixes of solvents were also used to optimize the solubility data (see Table S1 in SI). Table 2 and Figure 4 sum up the obtained HSP values.

MDI/BDO polymer shows higher polar and hydrogen bond components than the polyol resulting in a higher polarity for this polymer illustrated by its higher global solubility parameter compared to that of Radia 7285 polyol. Furthermore, the solubility sphere which encompasses all the good solvents (appearing as blue dots) and leaving the poor solvents outside (red dots), displays a higher radius for the polyol compared to MDI/BDO polymer (Figure 4 a and b) for which fewer good solvents are found (only two are included in the sphere, namely tetrahydrofuran (THF) and m-cresol) suggesting that MDI/BDO generally presents a limited solubility. These results should be compared with observations made previously from DSC analyses. The HS models are indeed highly crystalline at room temperature and this crystallinity can be explained by the existence of strong hydrogen bond and polar interactions between the MDI/BDO polymer chains. Therefore, it is consistent to observe a low solubility for this material.

In an attempt to evaluate miscibility between both blocks of the TPU, Figure **4**c compares the solubility sphere of the Radia 7285 polyol with that of MDI/BDO polymer. The good

overlapping of the spheres (95% of the hard segment sphere is included in the polyol sphere) with a HSP distance of 3.8 $MPa^{1/2}$ suggests a good miscibility between soft and hard blocks of the polymer. However, the previous DSC results show that phase separation is clearly occurring in the polymer microstructure as revealed by the signature of the low SS glass transition temperature and the HS melting. This phase separation is thus in fact favored by the ability to crystallize of the MDI/BDO hard segments. As polymerization takes place between T_g (about 50°C) and T_m (about 200°C) of the HS, crystallization of HS can occur as the reaction progresses, resulting in the formation of semi-crystalline HS domains. In addition, one has to remember that chain end HDO moieties are present in Radia 7285 and such HDO groups are expected to generate short MDI/HDO hard segments after reaction in the final structure of the TPU. These ones can change the actual thermodynamic contribution of both hard and soft phases in the polymer. Thus, the use of a model considering separately hard and soft segments to assess phase segregation in the TPU from Hansen solubility parameters is therefore not so adequate.

To overcome this discrepancy, the second approach considers the whole TPU to calculate the HSP values after testing its solubility in various solvents. HSPs of the TPU containing 13 wt% of HS were calculated using a double sphere fitting on HSPiP software considering the "Genetic Algorithm" calculation method[26]. It should be emphasized that both methods give a good fit for the HSP values (fit=1, meaning that the sphere encompasses only all the good solvents (blue dots), leaving the bad solvents (red dots) outside). We can then consider that each of the two spheres stands for hard and soft segments separately. As shown in Table 2, HSP of the soft segments are very close to those of the Radia 7285 polyol with only a slightly higher component dispersive and a lower hydrogen bond component compared to Radia 7285. In addition, a smaller radius is observed for the soft segment block sphere (Table 2 and Figure 4d). The reaction of MDI with the Radia 7285 polyol leads to the formation of urethane groups having a lower hydrogen bond component and a higher dispersive component due to the combined effect of the skeleton of MDI and the increasing molar mass. In addition, a significant decrease of the radius of the solubility sphere occurred with the presence of MDI in the TPU.

Regarding the hard segment block, its whole solubility parameter is much higher than that of MDI/BDO polymer, illustrating a higher polarity of the hard segments contained in the TPU (higher polar and hydrogen bond components). Generally speaking, the hard segments are more polar than the soft ones and display a lower radius of their solubility sphere. Figure **4**d shows that there is no overlapping between the solubility spheres of soft and hard blocks of the TPU, i.e. there is no compatibility between those components. In fact, a HSP distance of 8.4 $MPa^{1/2}$ between the two blocks confirms that there are not compatible which is in agreement with the thermal properties described previously.

Table 2. Hansen's solubility parameters.

Component	δ_{TOT} ($MPa^{1/2}$)	δ_D ($MPa^{1/2}$)	δ_P ($MPa^{1/2}$)	δ_H ($MPa^{1/2}$)	Sphere radius R_0 ($MPa^{1/2}$)
Radia 7285 polyol	20.2 ± 0.9	18.2 ± 0.5	4.2 ± 0.9	7.7 ± 0.5	6.5
MDI/BDO polymer	21.6 ± 1.1	17.7 ± 0.5	5.9 ± 1.2	10.9 ± 0.7	3.4
Soft segment (SS)	20.7 ± 0.9	19.1 ± 0.6	4.2 ± 0.9	6.7 ± 0.4	5.3
Hard segment (HS)	24.3 ± 1.5	18.2 ± 0.5	8.2 ± 1.7	13.8 ± 0.9	3.1

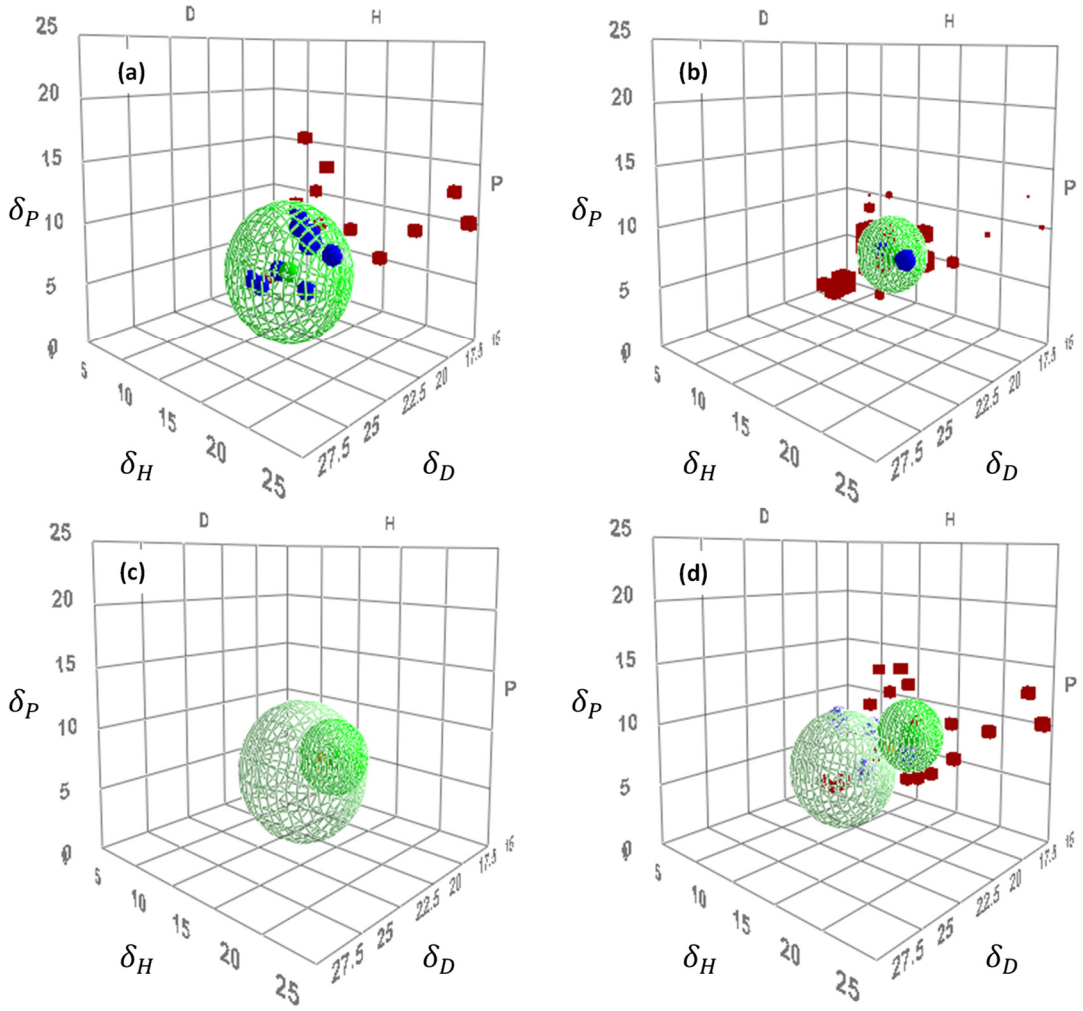

Figure 4. Solubility sphere diagrams ($\boldsymbol{\delta_D}\left(\boldsymbol{MPa^{\frac{1}{2}}}\right)$, $\boldsymbol{\delta_P}\left(\boldsymbol{MPa^{\frac{1}{2}}}\right)$, $\boldsymbol{\delta_H}$ $\left(\boldsymbol{MPa^{\frac{1}{2}}}\right)$) of a) Radia 7285 polyol, b) MDI/BDO polymer, c) comparison between Radia 7285 (light green) and MDI/BDO polymer spheres (green), d) TPU with soft (light green) and hard (green) segments . Blue dots and red dots stand for good and poor solvents, respectively (see online version for colour features).

It is also of interest to consider the solubility parameters of the different TPUs considered as homogeneous compounds. Table **3** gives the HSP values for TPU 8, TPU 13, and TPU 30 obtained with a single sphere fitting. Increasing hard segment content in TPU leads to higher global solubility parameters due to higher polar and hydrogen bond components and to a decrease in the solubility sphere radius. These results mean that at low HS content, the TPU displays a good overall solubility with numerous solvents (supporting information, Figure S5). It suggests that the TPU becomes more polar as the hard segment content increases due to the fact that the soft segment is often the less polar segment.

Table 3. Hansen's solubility parameters of TPU 8, TPU13, and TPU30.

Material	δ_{TOT} ($MPa^{1/2}$)	δ_D ($MPa^{1/2}$)	δ_P ($MPa^{1/2}$)	δ_H ($MPa^{1/2}$)	Sphere radius R_0 ($MPa^{1/2}$)
TPU 8	19.7 ± 0.4	17.9 ± 0.2	2.7 ± 0.5	7.7 ± 0.4	7.3
TPU 13	21.2 ± 0.6	18.1 ± 0.1	4.9 ± 1.0	9.8 ± 0.6	4.4
TPU 30	21.4 ± 0.5	17.5 ± 0.2	4.7 ± 0.5	11.3 ± 0.3	3.7

3.2. TPU morphologies

The multiscale morphology of the TPUs was characterized using TEM and AFM. Figure 5 shows TEM micrographs of the TPUs containing various hard segment contents. TEM demonstrates the existence of a continuous soft phase (brighter) containing small hard segments-rich domains (appearing darker due to their higher electronic density of the HS that are semi-crystalline). This presence is even more evidenced as the HS content increases, giving rise to the presence of spherulite-like entities (Figure 5a) and bigger hard segments-rich domains (Figure 5c). Figure 5c also shows that TPU 30 exhibits spherulite-like objects as three of them are present on the micrograph. These results confirm the phase separation occurring within the TPU as predicted by solubility parameter measurements and inferred from DSC analysis. Similar morphologies were previously evidenced by TEM and AFM microscopies on a TPU based on a dimer fatty acid derived polyol[4]. Figure 6 gives the AFM phase images highlighting the HS/SS phase separation in TPU 13 and TPU 30 (at a much smaller scale) (as confirmed by the corresponding height images in supporting information, Figure S 6). At high magnification (Figure 6b), one can observed for TPU 13, small hard domains well dispersed in the soft phase (hard phase appears brighter for such observation conditions) having a size close to 10 nm. At a lower magnification (Figure 6a), hard domains forming aggregates containing ramified arms in TPU 13 can be evidenced. Considering a higher HS content (TPU 30), a well-defined network of hard domains in the soft continuous phase is observed (Figure 6c).

As a result, the morphology of all the TPUs considered in this study is based on large hard segment-rich particles having a micrometer size at high HS content dispersed in a continuous soft segment-rich phase that contains nano-domains of hard segments, either dispersed or forming a seemingly percolating network.

Additional morphology investigations of polyurethanes using AFM have also reported the multiscale organization of the hard segments in the polymer[15,17,51,63]. Similar studies as that presented in this paper, show that at low HS content, the morphology is based on dispersed nano-size particles of hard segments and when increasing the HS content to 25 wt%, well defined domains of irregular shape form a hard segments-based network[64,65].

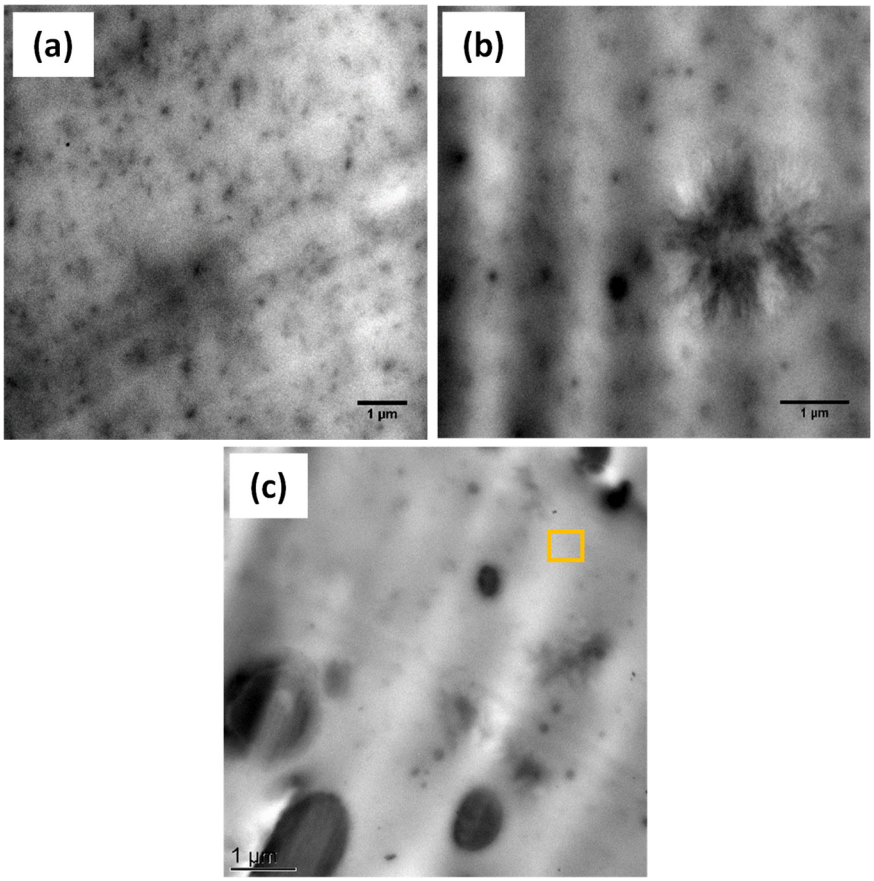

Figure 5. Transmission electron microscopy micrographs of a) TPU 13; b) TPU 15, and c) TPU30. The area in the yellow frame was then observed by AFM (see Fig. 6c).

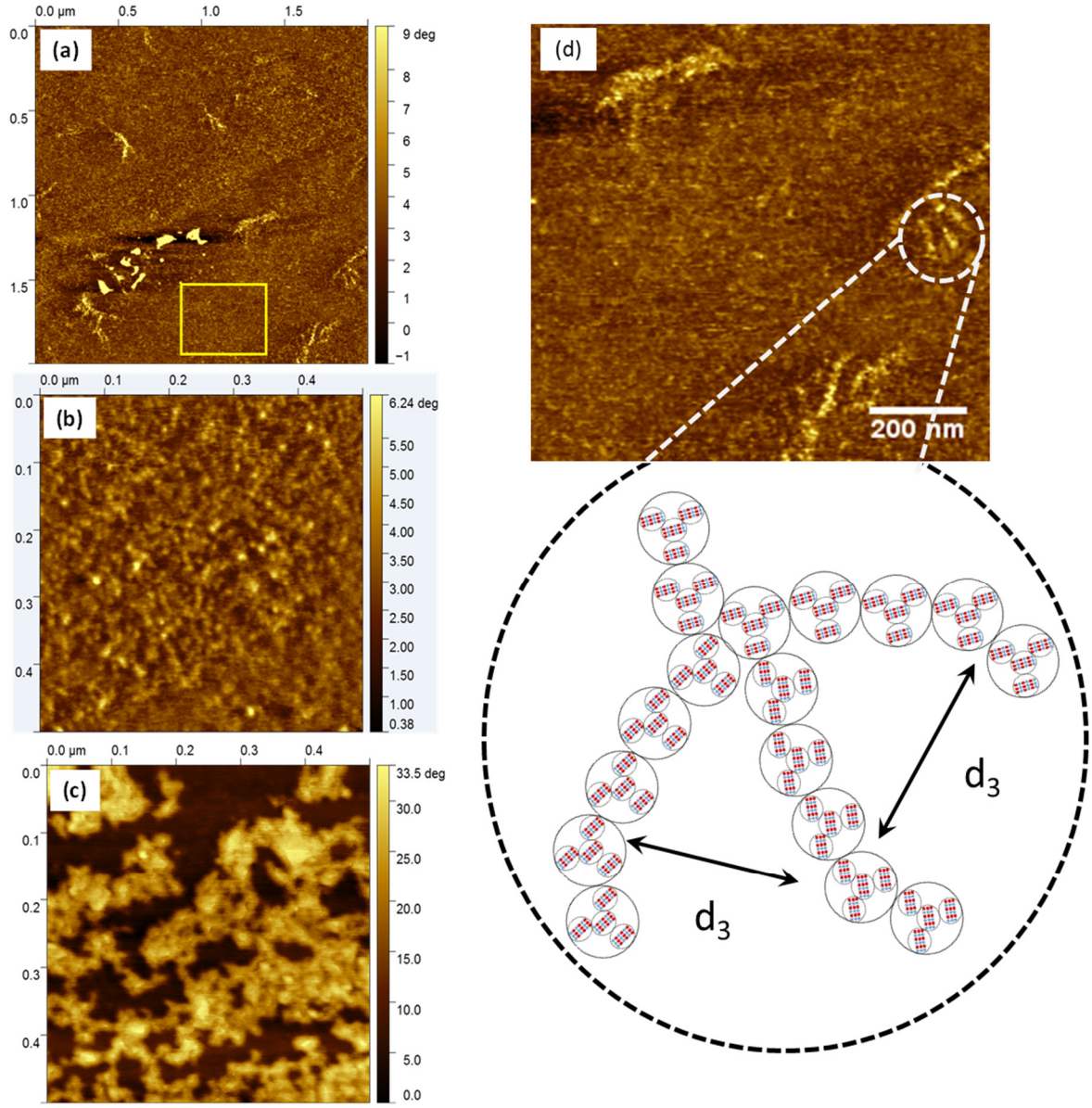

Figure 6. AFM phase images (hard phases brighter, soft phases darker) of a) TPU 13; b) TPU 13 at a higher magnification (zoom in from the yellow frame in Figure 6a)); c) TPU 30 observed in the yellow frame in Figure 5c; d) enlargement of 6a) showing distance d_3 (see below and Figure 7 for details of TPU microstructure)

Further investigations of the TPU morphology were made via small angle X-ray scattering analyses. Figure 7 shows SAXS patterns obtained for the TPU without BDO (Kratky's diagram, see supporting information, Figure S6). As previously mentioned, 8 wt% or even more of the hard segments in this polymer are issued from the reaction between MDI and the polyol chain ends composed of hexanediol moieties. Several peaks in the Porod' region are evidenced. At high q value, a small inflection at q_0 (2.4 nm^{-1}) corresponds to the hard segment sequence unit (HDO-MDI) of $d_0 = 2.6$ nm length according to the Bragg law. This value is close to the length of the MDI/HDO sequence reported in literature at 2.1 nm[16,66]. At lower q, the decrease in intensity in q^{-4} highlights the presence of larger,

hard, and dense dispersed particles with a sharp interface with the soft segments continuous phase. These ones are presumably based on few HS sequences, leading to the occurrence of a scattering peak at q_1 (8.2 nm^{-1}), corresponding to a dispersed phase diameter, d_1, (7.7 nm). At lower q value, the intensity evolves in q^{-2} and a correlation peak is observed at q_2 (0.46 nm^{-1}), corresponding to an inter-dispersed HS-rich particles correlation distance of $d_2 = 13.6$ nm. The q^{-2} slope evidences a ramified organization of these hard nodules. In the Guinier's regime, at very low q value, the q^{-4} slope demonstrates the presence of larger scattering objects having a smooth interface with the continuum, i.e. the continuous phase based on soft segments, which could correspond to larger hard segment-rich domains. The morphology analyzed by SAXS for TPUs is very close to the morphology of thermoplastic elastomer copolymers having soft and hard segments, as shown for instance on segmented polymers with poly(tetrahydrofuran) soft blocks and bis(terephthalate) diamide-based hard blocks[67].

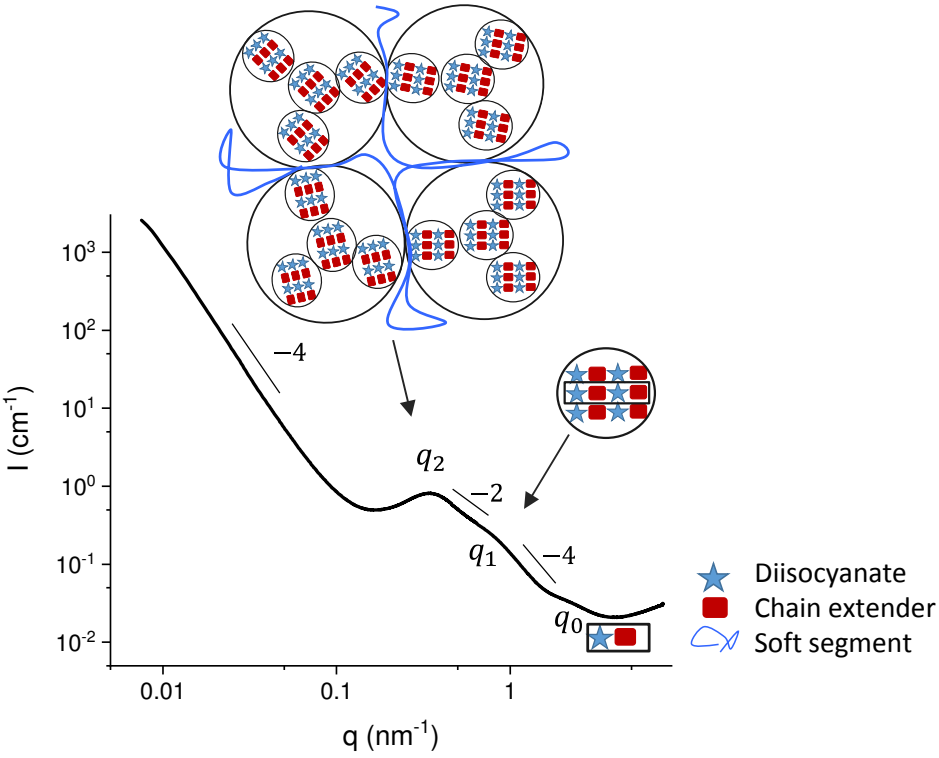

Figure 7. SAXS scattering profile for TPU8 (I=f(q)). A scheme of the proposed TPU microstructure is given.

Fernandez-d'Arlas *et al.* have shown for a poly(tetrahydrofuran)-based polyurethane that the correlation distance between HS domains corresponds to the average length of the polyol chain[11]. Based on a study from Koberstein *et al.* that reported a number of 3 or 4 HS sequences are required to create a hard domain[61], these authors assumed that two soft polyol chains are involved between hard domains and they calculated a correlation distance of 11-13 nm, in agreement with their experimental values[11]. Based on this study, the

distance of 7.7 nm observed could correspond to an average dimension of hard domains composed of 3 or more sequences of hard segments. The theoretical hard segment phase dimension , denoted d_1', is equal to $d_1' = n \times c - d_{HD}$, with $d_{HD} = 0.9\ nm$ the length of a hexanediol unit[68]. Considering a MDI/HDO crystal length of $c = 2.1\ nm$[16,66] for a hard segment dispersed phase composed of $n = 4$ MDI/HDO units, d_1' is found to be 7.5 nm in agreement with the experimental value of d_1. From the experimental correlation distance d_2 of 13.6 nm, a value close to 6.1 nm can be approximated for the length of a soft segment (d_{ss}) (Figure 8). Thus, it is assumed that the soft segment can contain one or more polyol chains.

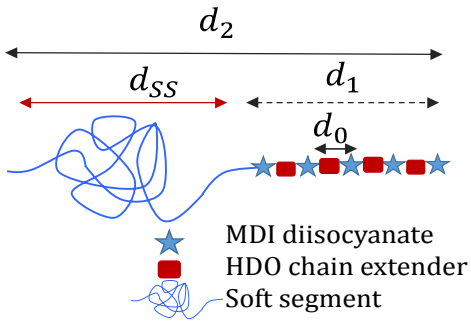

Figure 8. Schematic representation of the correlation distance observed by SAXS for TPU 8 (based on the work of Fernandez-d'Arlas *et al*[11]).

Figure 9 shows SAXS patterns for TPUs (see Figure S6 in SI for Kratky' plots). As expected, the scattering intensity depends on the HS content of the TPU. The higher the HS content, the higher the intensity. In a similar way to what has been previously discussed for TPU 8, hard nodule size (d_1) and correlation distances calculated with Bragg' law are summarized in Table 4 for TPU containing MDI/BDO hard segments, in addition to those formed with MDI/HDO of the polyol chain ends. Considering TPU 13 and TPU 15, the size of the hard segments-rich domains appeared to be lower than the one of TPU 8. This phenomenon can be explained by the difference of hard segment sequence lengths between BDO and HDO-based ones. In fact, MDI/BDO has a crystal sequence length of 1.9 nm[16,66] which is slightly lower than MDI/HDO (2.1 nm). For these polymers, a small inflection appears at a lower q value, q_3 (0.2 nm^{-1}) (Figure 9). It is assumed that the hard domains can assemble as ramified aggregates as observed in the AFM phase image of TPU 13 at low magnification (Figure 6a). The associated distance d_3 could correspond to the average distance between arms of these ramified objects (Figure 6d). At very low q value, the slope of the SAXS pattern for TPU 13 and TPU 15 is higher than -3 which confirms the presence of ramified scattering objects having a fractal interface with the continuous soft phase medium. Considering TPU 20, TPU 25, and TPU 30, only two peaks are observed on the patterns, the correlation distances d_2 and d_3. The shape factor of the dispersed objects, associated with the q_1 peak is no longer visible. Then, it is assumed that both q_1 and q_2 peaks appear at close q values, giving rise to the presence of a unique peak. This can be explained by the fact that the dispersed objects are more and more densely packed within the TPU and are assumed to be in close contact for the highest HS contents. This effect was previously

revealed by AFM phase image for TPU 30 (Figure 6c) where the aggregation of the hard domains leads to a dense percolated network. From 13 to 30 wt% of hard segments in the TPU, the correlation distance d_2 increases in agreement with the increase in the size of the hard domains. A decrease in the correlation distance d_3 is also observed when increasing HS content from 20 to 30 wt%. Literature reports similar results for this additional correlation distance which was attributed to lamellar interdomain distance[69]. Koberstein and Stein[69] explained the decrease of d_3 by the folding of the hard segment chains due to butanediol flexible chain leading to a constant lamellar thickness.

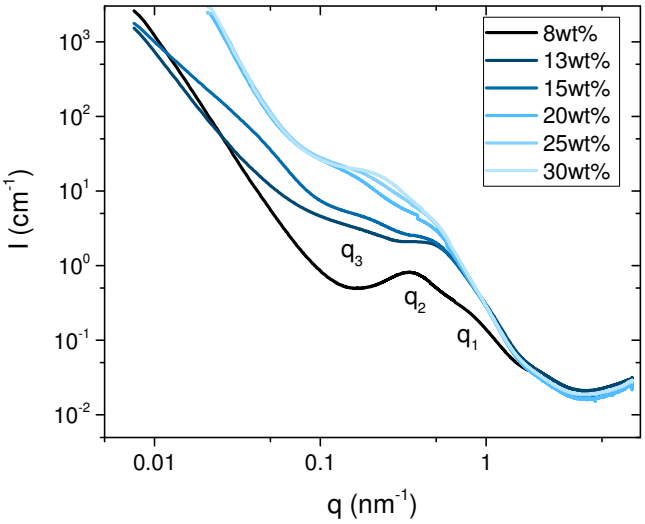

Figure 9. SAXS scattering intensity I=f(q) of TPUs as a function of hard segment content.

Table 4. Characteristic distances revealed by SAXS spectra.

MDI/BDO HS content (wt%)	**d_0 (nm)**	**d_1 (nm)**	**d_2 (nm)**	**d_3 (nm)**
13	2.6	7.0	11.0	31.4
15	2.6	7.0	11.7	31.0
20	2.6	-	12.5	33.7
25	2.6	-	14.7	29.6
30	2.6	-	14.3	21.5

From all these conclusions regarding the organization of the polymer at the nano and micro scales, Figure **10** illustrates: *i/* the phase separation occurring between hard and soft segments in the microstructure of the TPU due to incompatibility between these two blocks (according to thermal characterization, solubility parameters, and microstructural analyses); *ii/* the ability of hard segments to form either long chains at high hard segment content or isolated hard segments which can plasticize the long hard segment chains (see the increase

of T_g in Figure **3**); *iii*/ well organized hard segments within crystal-like structure at high hard segment content.

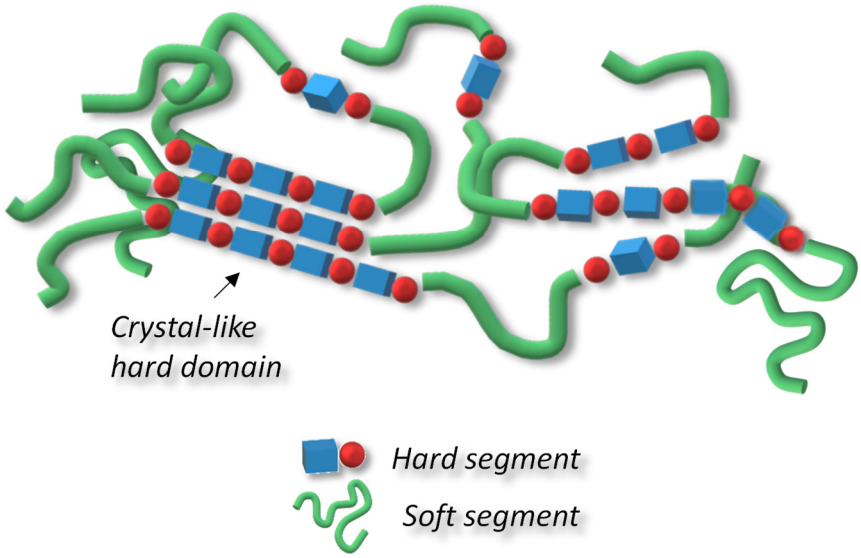

Figure 10. Scheme illustrating phase separation between hard and soft segments in the microstructure of TPU.

3.3. Thermomechanical properties

Thermomechanical properties were evaluated by combined isochronal curves of storage shear modulus, G', and loss factor, tan δ, at 1 Hz for all TPUs having various HS contents. Figure 11 shows G' and tan δ for TPUs containing 8 to 30 wt% HS. As previously observed for the T_g of the TPUs by thermal analysis, all the TPUs display a main relaxation associated with T_g in the same temperature range, i.e. from -45 to 40°C (Figure **1**).

At higher temperature, the TPU mechanical behavior depends on the HS content. Regarding SAXS analysis (Figure **9**), TPU 8 contains very few hard segments that form hard nanodomains well dispersed within the microstructure of the polymer which might act as physical crosslinking nodes in the soft segments continuous rich phase. These small hard domains in addition to physical entanglements confer a thermoplastic elastomer mechanical behavior to TPU 8, illustrated by a narrow rubbery plateau before flow after relaxation of the hard domains close to 39°C.

TPU 13 and TPU 15 show intermediate behaviors with broader rubbery and higher plateau compared to TPU 8. Two phenomena can explain these results: *i*/ an increase in the hard segment chain length leading to higher glass transition for the hard domains (see DSC analyses) and allowing the polymer to flow at a higher temperature; *ii*/ hard domains forming ramified arms in the microstructure of the polymers (see Figure 6 and SAXS data) acting as small reinforcing ramified objects.

The difference between TPU 13 and TPU 15 can be explained by the semi-crystalline nature of HS. Indeed, spherulite-like objects have been observed for TPU 15 (see TEM image in Figure 5) associated with the appearance of a melting temperature evidenced by DSC. These objects can also act as reinforcing fillers for the soft continuous phase in addition to the hard domains. Moreover, TPU 15 does not flow above the relaxation of the HS but only after melting of the crystallized hard segments, i.e. from 150 to 210°C (Figure **1**).

At higher HS content, TPU 20, TPU 25, and TPU 30 show an extended rubbery plateau with a high storage modulus which could be explained by the presence of bigger hard domains (see SAXS and TEM). A compact and percolated network based on these semi-crystalline hard domains is formed and acts as a mechanically effective structure up to their melting close to 170°C. For these TPUs, a small inflection is also evidenced from 50 to 130°C on G' which is associated with a slight shoulder on tan δ (Figure **11**b). This can be attributed to the main relaxation of the hard segment amorphous phase, as previously highlighted by DSC (Figure 2).

As a result, increasing HS content in the TPU from 13 to 30 wt% leads to an increase in storage modulus in the rubbery state (from 1 to 5 MPa at 50°C). Literature has reported the same behavior for polyurethanes containing MDI/BDO as hard segments and polybutadiene[10], polycaprolactone[9], or fatty acid derived polyol[4] as soft segments. This reinforcement effect is known in linear block copolymers and has been recently well described in literature on segmented copolymers having diamides as hard blocks[70].

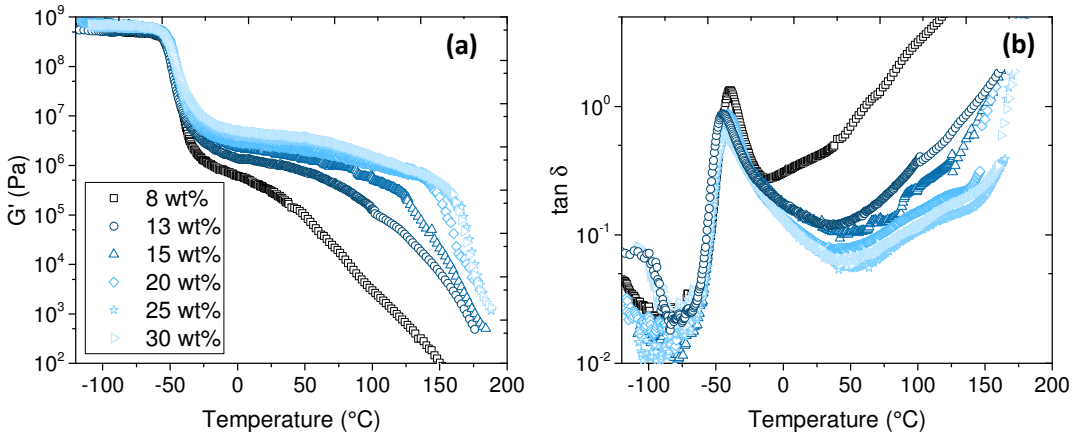

Figure 11. Dependence of G' and tan δ of TPUs having different hard segment content.

4. Conclusions

In this work, we intended to highlight the importance to consider the thermodynamics to predict and tailor (nano/micro)phase separation phenomena in thermoplastic polyurethanes (TPU) by using Hansen' solubility parameters. Therefore HSP have been accurately measured for MDI/BDO hard segments and the fatty acid derived soft segment

which were considered for design a series of TPUs having various hard segment contents. By using the HSPiP software, the construction of the solubility spheres for both soft and hard segments revealed that these two compounds taken separately show incompatibility. This conclusion was confirmed for the different types of TPUs from the observed increase of the T_g and a high segregation degree between HS and SS measured by DSC. On the other hand, by considering the same HSP-based approach to TPUs, we have shown that their overall solubility, i.e. the radius of their average solubility sphere, strongly decreases with the HS content. Moreover, the solubility diagram of these materials can also be well described by a two spheres model. The latter one considers that, once HS and SS incorporated in the TPUs as constitutive blocks, the TPUs can be described as a two non-miscible phases based materials. By combining these results with thermal analysis and morphological characterizations, we can assume that these two phases could be described as: *i)* the soft phase consisting of polyol chains and some short miscible hard segments having a molar masses distribution which increases with the HS content; *ii)* the non-miscible hard segments organized as semi-crystalline nanodomains dispersed within the soft phase, themselves being able to assemble in the form of ramified objects that can percolate at high HS contents. This nanostructuration provides a TPE-like thermomechanical behavior to the TPUs assessed by the presence of a rubbery plateau up to HS melting in addition to a reinforcement effect from HS objects.

This study also proposes a tool to describe TPUs by coupling HSP and morphology characterizations. This approach allows a good understanding of the formation of the nanostructures in TPUs and a better understanding of their mechanical behavior. This constitutes a robust predictive tool for predicting the miscibility of TPUs with other components. This work allows to design macromolecular architectures of TPUs for given targeted properties.

Author contributions

All authors have contributed to the writing of the manuscript and have given approval for its final version.

Notes

The authors declare no competing financial interest for this work.

Acknowledgements

The authors express their thanks to Soprema Co. and Eiffage Infrastructures Co. for their financial support and to Professor Jean-Pierre Pascault for helpful discussions and advice. Dr Catherine Ladavière (IMP) is gratefully acknowledged for the MALDI-TOF analysis.

The authors would also like to thank the NMR Polymer Center of the "Institut de Chimie de Lyon" (FR3023), for assistance and access to the NMR facilities. The "Centre Technologique des Microstructures, plateforme de l'Université Claude Bernard Lyon 1", CTμ is acknowledged for granting access to their equipment.

Appendix. Definitions of parameters used

T_g	Glass transition
ΔG_M	Change of free enthalpy
χ	Interaction parameter
V_{ref}	Reference volume
Φ	Volume fraction
δ	Solubility parameter
δ_D	Dispersive component of solubility parameter
δ_P	Polar component of solubility parameter
δ_H	Hydrogen bond component of solubility parameter
E	Cohesive energy
V	Molar volume
ΔC_p	Isobaric heat capacity
G‘	Storage modulus
tan δ	Loss factor
I	Scattering intensity
q	Scattering vector
d	Interdomain spacing

References

[1] M.F. Sonnenschein, Polyurethanes: Science, Technology, Markets, and Trends, Hoboken, John Wiley & Sons, Inc, New Jersey, USA, 2015.

[2] E. Delebecq, J.P. Pascault, B. Boutevin, F. Ganachaud, On the versatility of urethane/urea bonds⊚: Reversibility, blocked isocyanate, and non-isocyanate polyurethane, Chem. Rev. 113 (2013) 80–118. https://doi.org/10.1021/cr300195n.

[3] M. Charlon, B. Heinrich, Y. Matter, E. Couzigné, B. Donnio, L. Avérous, Synthesis, structure and properties of fully biobased thermoplastic polyurethanes, obtained from a diisocyanate based on modified dimer fatty acids, and different renewable diols, Eur. Polym. J. 61 (2014) 197–205. https://doi.org/10.1016/j.eurpolymj.2014.10.012.

[4] H. Blache, F. Méchin, A. Rousseau, É. Fleury, J.-P. Pascault, P. Alcouffe, N. Jacquel, R. Saint-Loup, New bio-based thermoplastic polyurethane elastomers from isosorbide and rapeseed oil derivatives, Ind. Crops Prod. 121 (2018) 303–312. https://doi.org/10.1016/j.indcrop.2018.05.004.

[5] T. Calvo-Correas, M.D. Martín, A. Retegi, N. Gabilondo, M.A. Corcuera, A. Eceiza, Synthesis and characterization of polyurethanes with high renewable carbon content and tailored properties, ACS Sustainable Chem. Eng. 4 (2016) 5684–5692. https://doi.org/10.1021/acssuschemeng.6b01578.

[6] A. Saiani, C. Rochas, G. Eeckhaut, W.A. Daunch, J.W. Leenslag, J.S. Higgins, Origin of multiple melting endotherms in a high hard block content polyurethane . 2 . Structural investigation, Macromolecules 37 (2004) 1411–1421. https://pubs.acs.org/doi/abs/10.1021/ma034604+.

[7] A. Saiani, W.A. Daunch, H. Verbeke, J.-W. Leenslag, J.S. Higgins, Origin of multiple melting endotherms in a high hard block content polyurethane. 1. Thermodynamic investigation, Macromolecules 34 (2001) 9059–9068. https://doi.org/10.1021/ma0105993.

[8] Y. Camberlin, J.P. Pascault, Quantitative DSC evaluation of phase segregation rate in linear segmented polyurethanes and polyurethaneureas, J. Polym. Sci. Polym. Chem. Ed. 21 (1983) 415–423. https://doi.org/10.1002/pol.1983.170210211.

[9] C.G. Seefried, J. V. Koleske, F.E. Critchfield, Thermoplastic urethane elastomers. III. Effects of variations in hard-segment concentration, J. Appl. Polym. Sci. 19 (1975) 2503–2513. https://doi.org/10.1002/app.1975.070190913.

[10] L. Cuvé, J.P. Pascault, G. Boiteux, Synthesis and properties of polyurethanes based on polyolefin©: 2 . Semicrystalline segmented polyurethanes prepared under heterogeneous or homogeneous synthesis conditions, Polymer 33 (1992) 3957–3967. https://doi.org/10.1016/0032-3861(92)90389-E.

[11] B. Fernández-D'Arlas, J. Balko, R.P. Baumann, E. Pöselt, R. Dabbous, B. Eling, T. Thurn-Albrecht, A.J. Müller, Tailoring the morphology and melting points of segmented thermoplastic polyurethanes by self-nucleation, Macromolecules 49 (2016) 7952–7964. https://doi.org/10.1021/acs.macromol.6b01527.

[12] J. Foks, G. Michler, I. Nauman, Determination of lamellae in segmented polyurethanes by electron microscopy, Polymer 28 (1987) 2195–2199. https://doi.org/10.1016/0032-3861(87)90375-2.

[13] C. Li, S.L. Cooper, Direct observation of the micromorphology of polyether polyurethanes using high-voltage electron microscopy, Polymer 31 (1990) 3–7. https://doi.org/10.1016/0032-3861(90)90339-Z.

[14] C. Li, S.L. Goodman, R.M. Albrecht, S.L. Cooper, Morphology of segmented polybutadiene-polyurethane elastomers, Macromolecules 21 (1988) 2367–2375. https://doi.org/10.1021/ma00186a012.

[15] E. Tocha, H. Janik, M. Debowski, G.J. Vancso, Morphology of polyurethane revisited by complementary AFM and TEM, J. Macromol. Sci. Part B. 41 (2002) 1291–1304. https://doi.org/10.1081/MB-120013098.

[16] J. Blackwell, C.D. Lee, Hard-segment polymorphism in MDI/Diol-based polyurethane elastomers, J. Polym. Sci. Polym. Phys. Ed. 22 (1984) 759–772. https://doi.org/10.1002/pol.1984.180220417.

[17] A. Aneja, G.L. Wilkes, A systematic series of 'model' PTMO based segmented polyurethanes reinvestigated using atomic force microscopy, Polymer 44 (2003) 7221–7228. https://doi.org/10.1016/j.polymer.2003.07.007.

[18] L.A. Utracki, C.A. Wilkie, Polymer Blends Handbook. Second edition, Springer, 2014. https://doi.org/10.1007/978-94-007-6064-6.

[19] E. Manias, L.A. Utracki, Thermodynamics of polymer blends, Springer, Dordrecht, 2014. https://doi.org/10.1007/978-94-007-6064-6_4.

[20] P. Peng, B. Shi, L. Jia, B. Li, Relationship between Hansen Solubility Parameters of ABS and its Homopolymer Components of PAN , PB , and PS, J. Macromol. Sci. Part B Phys. 49 (2010) 864–869. https://doi.org/10.1080/00222341003603693.

[21] L. Leibler, Theory of microphase separation in block copolymers, Macromolecules 13 (1980) 1602–1617. https://doi.org/10.1021/ma60078a047.

[22] V. V Ginzburg, J. Bicerano, C.P. Christenson, A.K. Schrock, A.Z. Patashinski, Theoretical Modeling of the relationship between Young's modulus and formulation variables for segmented polyurethanes, J. Polym. Sci. Part B Polym. Phys. 45 (2007) 2123–2135. https://doi.org/10.1002/polb.

[23] I. Yilgör, E. Yilgör, G.L. Wilkes, Critical parameters in designing segmented polyurethanes and their effect on morphology and properties: A comprehensive review, Polymer 58 (2015) A1–A36. https://doi.org/10.1016/j.polymer.2014.12.014.

[24] Y. Camberlin, J.P. Pascault, Phase segregation kinetics in segmented linear polyurethanes : Relations between equilibrium time and chain mobility and between equilibrium degree of segregation and interaction parameter, J. Polym. Sci. Polym. Phys. Ed. 22 (1984) 1835–1844. https://doi.org/10.1002/pol.1984.180221011.

[25] C.M. Hansen, Hansen solubility parameters: a user's handbook, Second Edition, Taylor & Francis Group, Boca Raton, 2007.

[26] C.M. Hansen, The three dimensional solubility parameter and solvent diffusion coefficient. Their importance in surface coating formulation, Danish Technical Press, Copenhagen, 1967.

[27] C.M. Hansen, The universality of solubility parameter, Ind. Eng. Chem. Prod. Res. Dev. 8 (1969) 1–11. https://doi.org/10.1111/j.1471-6402.1998.tb00179.x.

[28] S. Abbott, C.M. Hansen, H. Yamamoto, Hansen Solubility Parameters in Practice complete with eBook , software and data 5th edition, 2013.

[29] K.W. Suh, J.M. Corbett, Solubility parameters of polymers from turbidimetric titrations, J. Appl. Polym. Sci. 12 (1968) 2359–2370. https://doi.org/10.1002/app.1968.070121012.

[30] R. Mieczkowski, Solubility parameter components of some polyurethanes, Eur. Polym. J. 28 (1992) 53–55. https://doi.org/10.1016/0014-3057(92)90237-V.

[31] R. Mieczkowski, Solubility parameter components of some polyols, Eur. Polym. J. 27 (1991) 377–379. https://doi.org/10.1016/0014-3057(91)90191-P.

[32] P.G. Redelius, Solubility parameters and bitumen, Fuel 79 (2000) 27–35. https://doi.org/10.1016/S0016-2361(99)00103-9

[33] J. Camacho, E. Díez, I. Díaz, G. Ovejero, Hansen solubility parameter: from polyethylene and poly(vinyl acetate) homopolymers to ethylene–vinyl acetate copolymers, Polym. Int. 66 (2017) 1013–1020. https://doi.org/10.1002/pi.5351.

[34] E. Díez, G. Ovejero, M.D. Romero, I. Díaz, Polymer-solvent interaction parameters of SBS rubbers by inverse gas chromatography measurements, Fluid Phase Equilib. 308 (2011) 107–113. https://doi.org/10.1016/j.fluid.2011.06.018.

[35] D. Pospiech, A. Gottwald, D. Jehnichen, P. Friedel, A. John, C. Harnisch, D. Voigt, G. Khimich, A.Y. Bilibin, Determination of interaction parameters of block copolymers containing aromatic polyesters from solubility parameters obtained from solution viscosities, Colloid Polym. Sci. 280 (2002) 1027–1037. https://doi.org/10.1007/s00396-002-0728-6.

[36] P. Redelius, Bitumen solubility model using Hansen solubility parameter, Energy Fuels 18 (2004) 1087–1092. https://doi.org/10.1021/ef0400058.

[37] J. Bonnet, G. Suissa, M. Raynal, L. Bouteiller, Organogel formation rationalized by Hansen solubility parameters: Dos and don'ts, Soft Matter 10 (2014) 3154–3160. https://doi.org/10.1039/c4sm00244j.

[38] D. Rosa Nunes, M. Raynal, B. Isare, P.A. Albouy, L. Bouteiller, Organogel formation rationalized by Hansen solubility parameters: Improved methodology, Soft Matter 14 (2018) 4805–4809. https://doi.org/10.1039/c8sm00562a.

[39] D.J. David, T.F. Sincock, Estimation of miscibility of polymer blends using the solubility parameter concept, Polymer 33 (1992) 4505–4514. https://doi.org/10.1016/0032-3861(92)90406-M.

[40] P. Furtwengler, R. Matadi Boumbimba, A. Sarbu, L. Avérous, Novel Rigid Polyisocyanurate Foams from Synthesized Biobased Polyester Polyol with Enhanced Properties, ACS Sustainable Chem. Eng. 6 (2018) 6577–6589. https://doi.org/10.1021/acssuschemeng.8b00380.

[41] C. Zhang, M.R. Kessler, Bio-based polyurethane foam made from compatible blends of vegetable-oil-based polyol and petroleum-based polyol, ACS Sustainable Chem. Eng. 3 (2015) 743–749. https://doi.org/10.1021/acssuschemeng.5b00049.

[42] Y. Li, Z. Ren, M. Zhao, H. Yang, B. Chu, Multiphase structure of segmented polyurethanes: Effects of hard-segment flexibility, Macromolecules 26 (1993) 612–622. https://doi.org/10.1021/ma00056a010.

[43] J.E. Mark, Polymer data handbook, Oxford University Press, 1999.

[44] H. Sautel, P.E. Bindschedler, R. Perrin, Granules comprising bitumen and a thermoplastic polyurethane elastomer, method for its preparation and its uses. Soprema, US Patent 2015/0291798 (2015).

[45] D. Nečas, P. Klapetek, Gwyddion: An open-source software for SPM data analysis. Central European Journal of Physics, (2012) 10(1), 181–188. https://doi.org/10.2478/s11534-011-0096-2.

[46] E.C. Leonard, Polymerization-Dimer Acids, J. Am. Oil Chem. Soc. 56 (1979) 782A-785A. https://doi.org/10.1007/BF02667445.

[47] D.H. McMahon, E.P. Crowell, Characterization of products from clay catalyzed polymerization of tall oil fatty acids, J. Am. Oil Chem. Soc. 51 (1974) 522–527. https://doi.org/10.1007/BF02636021.

[48] A. Köckritz, A. Martin, Oxidation of unsaturated fatty acid derivatives and vegetable oils, Eur. J. Lipid Sci. Technol. 110 (2008) 812–824. https://doi.org/10.1002/ejlt.200800042.

[49] C. Bueno-Ferrer, E. Hablot, F. Perrin-Sarazin, M.C. Garrigós, A. Jiménez, L. Avérous, Structure and morphology of new bio-based thermoplastic Polyurethanes obtained from dimeric fatty acids, Macromol. Mater. Eng. 297 (2012) 777–784. https://doi.org/10.1002/mame.201100278.

[50] J. Balko, B. Fernández-D'Arlas, E. Pöselt, R. Dabbous, A.J. Müller, T. Thurn-Albrecht, Clarifying the origin of multiple melting of segmented thermoplastic polyurethanes by fast scanning calorimetry, Macromolecules 50 (2017) 7672–7680. https://doi.org/10.1021/acs.macromol.7b00871.

[51] B. Imre, H. Gojzewski, C. Check, R. Chartoff, C.J. Vancso, Properties and phase structure of polycaprolactone-based segmented polyurethanes with varying hard and soft segments: effects of processing conditions, Macromol. Chem. Phys. 219 (2018, 1700214. https://doi.org/10.1002/macp.201700214.

[52] L. Cuvé, J.P. Pascault, G. Boiteux, G. Seytre, Synthesis and properties of polyurethanes based on polyolefine : 1 . Rigid polyurethanes and amorphous segmented polyurethanes prepared in polar solvents under homogeneous conditions, Polymer 32 (1991) 343–352. https://doi.org/10.1016/0032-3861(91)90024-D.

[53] B. Bengtson, C. Feger, W.J. MacKnight, N.S. Schneider, Thermal and mechanical properties of solution polymerized segmented polyurethanes with butadiene soft segments, Polymer 26 (1985) 895–900. https://doi.org/10.1016/0032-3861(85)90134-X.

[54] B. Fu, C. Feger, W.J. MacKnight, N.S. Schneider, Synthesis and properties of monodisperse hydroxy-terminated oligomers of 1,4-butanediol and 2,4-toluene diisocyanate, Polymer 26 (1985) 889–894. https://doi.org/10.1016/0032-3861(85)90133-8.

[55] L.H. Peebles, Sequence Length Distribution in Segmented Block Copolymers, Macromolecules 7 (1974) 872-882. https://doi.org/10.1021/ma60042a034.

[56] L.H. Peebles, Hard block length distribution in segmented block copolymers, Macromolecules 9 (1976) 58–61. https://doi.org/10.1021/ma60049a010.

[57] J. Blackwell, K.H. Gardner, Structure of the hard segments in polyurethane elastomers, Polymer 20 (1979) 13–17. https://doi.org/10.1016/0032-3861(79)90035-1.

[58] L. Born, J. Crone, H. Hespe, E.H. Müller, K.H. Wolf, On the structure of polyurethane hard segments based on MDI and butanediol-1,4: X-ray diffraction analysis of oriented elastomers and of single crystals of a model compound, J. Polym. Sci. Polym. Phys. Ed. 22 (1984) 163–173. https://doi.org/10.1002/pol.1984.180220202.

[59] J.T. Koberstein, R.S. Stein, Small-angle light scattering studies of macrophase separation in segmented polyurethane block copolymers, Polymer 25 (1984) 171–177. https://doi.org/10.1016/0032-3861(84)90323-9.

[60] Y. Swolfs, E. Bertels, I. Verpoest, B. Goderis, Linking the morphology of a high hard segment content polyurethane to its thermal behaviour and mechanical properties, Polymer 81 (2015) 1–11. https://doi.org/10.1016/j.polymer.2015.11.007.

[61] A. Saiani, A. Novak, L. Rodier, G. Eeckhaut, J.-W. Leenslag, J.S. Higgins, Origin of multiple melting endotherms in a high hard block content polyurethane: Effect of annealing temperature, Macromolecules 40 (2007) 7252–7262. https://doi.org/10.1021/ma070332p.

[62] J.T. Koberstein, A.F. Galambos, L.M. Leung, Compression-molded polyurethane block copolymers. 1. Microdomain morphology and thermomechanical properties, Macromolecules 25 (1992) 6195–6204. https://doi.org/10.1021/ma00049a017.

[63] C. Check, B. Imre, H. Gojzewski, R. Chartoff, C.J. Vancso, Kinetic aspects of formation and processing of polycaprolactone polyurethanes in situ from a blocked isocyanate, Polym. Chem. 9 (2018) 1983-1995. https://doi-org.inc.bib.cnrs.fr/10.1039/C7PY02006F.

[64] V. Solouki Bonab, I. Manas-Zloczower, Revisiting thermoplastic polyurethane, from composition to morphology and properties, J. Polym. Sci. Part B Polym. Phys. 55 (2017) 1553–1564. https://doi.org/10.1002/polb.24413.

[65] S. Abouzahr, G.L. Wilkes, Z. Ophir, Structure-property behaviour of segmented polyether-MDI-butanediol based urethanes: effect of composition ratio, Polymer 23 (1982) 1077–1086. https://doi.org/10.1016/0032-3861(82)90411-6.

[66] J. Blackwell, M.R. Nagarajan, T.B. Hoitink, Structure of polyurethane elastomers : effect of chain extender length on the structure of MDI / diol hard segments, Polymer 23 (1982) 950–956. https://doi.org/doi:10.1016/0032-3861(82)90392-5.

[67] G.P. Baeza, A. Sharma, A. Louhichi, L. Imperiali, W.P.J. Appel, C.F.C. Fitié, M.P. Lettinga, E. Van Ruymbeke, D. Vlassopoulos, Multiscale organization of thermoplastic elastomers with varying content of hard segments, Polymer 107 (2016) 89–101. https://doi.org/10.1016/j.polymer.2016.11.010.

[68] J. Blackwell, M.R. Nagarajan, T.B. Hoitink, Structure of polyurethane elastomers. X-ray diffraction and conformational analysis of MDI-propandiol and MDI-ethylene glycol hard segments, Polymer 22 (1981) 1534–1539. https://doi.org/10.1016/0032-3861(81)90325-6.

[69] J.T. Koberstein, R.S. Stein, Small-angle X-ray scattering studies of microdomain structure in segmented polyurethane elastomers, J. Polym. Sci. Polym. Phys. Ed. 21 (1983) 1439–1472. https://doi.org/10.1002/pol.1983.180210814.

[70] G.P. Baeza, The Reinforcement effect in well-Defined segmented copolymers : Counting the topological constraints at the mesoscopic scale, Macromolecules 51 (2018) 1957–1966. https://doi.org/10.1021/acs.macromol.7b02208.